

Event-by-Event Physics in ALICE

Chiara Zampolli* for the ALICE Collaboration

Museo Storico della Fisica e Centro Studi e Ricerche Enrico Fermi (Roma) & INFN (Bologna)

E-mail: Chiara.Zampolli@bo.infn.it

Event-by-Event (E-by-E) fluctuations are one of the main dynamical probes of the phase transition from ordinary hadronic matter to a plasma of quarks and gluons, which is expected to occur in ultra-relativistic heavy-ion collisions. In this article, the results of a study concerning the observability of E-by-E fluctuations for the ALICE experiment at the LHC collider at CERN is presented. In particular, an estimate of the ALICE E-by-E statistical sensitivity in the measurement of the mean transverse momentum of charged hadrons, of the inverse slope parameter from the hadron transverse momentum spectra, and of their particle ratios is discussed. The analysis relies on the excellent performance of ALICE in terms of particle identification.

*The 2nd edition of the International Workshop — Correlations and Fluctuations in Relativistic Nuclear Collisions —
July 7-9 2006
Galileo Galilei Institute, Florence, Italy*

*Speaker.

1. Introduction

QCD lattice calculations predict that at very high temperature and energy density conditions a phase transition from the ordinary hadronic matter to a deconfined state of quarks and gluons (the so-called Quark-Gluon Plasma, QGP) should occur. The nature of this phase transition (especially the order of the phase transition, and even whether this is more a crossover rather than a sharp phase transition) and the existence of a (tri)critical end point are, however, topics still under discussion, where many parameters are involved, such as the value of the quark masses and of the baryochemical potential μ_B .

The heavy-ion physics program of the Large Hadron Collider (LHC) at CERN will concern Pb+Pb collisions at a centre-of-mass energy $\sqrt{s_{NN}} = 5.5$ TeV, making it possible to investigate the unexplored regime of extreme energy densities ($\epsilon = 15 - 40$ GeV/fm³), and high temperatures ($\mu_B \ll T$), where no sharp boundary is expected to show up between the hadronic matter and the QGP. The nature and the time evolution of the hot and dense system created in a heavy-ion collision will carry on the fingerprints of the QGP phase transition, which nonetheless may vary even dramatically from one event to the other. For this reason, an analysis on an Event-by-Event (E-by-E) basis will offer the opportunity to study the QCD phase transition and to get insights into the QGP.

Apart from the statistical fluctuations due to the geometrical properties of the collision [1, 2, 3], E-by-E fluctuations may be related to the thermodynamics of the system (such as the temperature [4, 5]), to fluctuations of conserved quantities (such as the charge [6]), to jets and minijets [7], and also to more exotic phenomena (such as Disoriented Chiral Condensate formation [8]).

ALICE (A Large Ion Collider Experiment) will be the experiment at the LHC aimed at investigating the phase transition and the QGP in heavy-ion collisions. Its physics program will span over a large number of observables, from the global properties of the collisions (multiplicities, rapidity distributions,...), to more selective QGP signals (direct photons, charmonium and bottomonium,...). Moreover, thanks to the very high number of particles produced in each collision, and relying on its excellent particle identification capabilities, ALICE will also perform event-by-event analyses.

In this paper, the ALICE E-by-E statistical sensitivity in measuring identified particle transverse momentum spectra and particle ratios (K/π , p/π) will be presented. In Section 2, the Monte Carlo event sample used for the analysis will be described. Sec. 3 will deal with the ALICE particle identification capabilities, fundamental as far as identified particle p_T spectra and particle ratios are concerned. Section 4 will present the results of the analyses on the mean p_T ($\overline{p_T}$) distributions (Sec. 4.2), on the inverse slope parameter from p_T spectra for identified pions, kaons and protons (Sec. 4.3), and for K/π and p/π ratios (Sec. 4.4). Finally, in the last section, the summary and the conclusions will be provided.

2. Monte Carlo Event Sample

The Monte Carlo event sample used for this analysis consists of 300 Pb+Pb central collisions at $\sqrt{s_{NN}} = 5.5$ TeV generated with the standard HIJING 1.36 Monte Carlo generator¹ [9]. The impact parameter has been chosen to be in the range $0 < b < 5$ fm, corresponding to 10% of the

¹The standard HIJING Monte Carlo generator includes the jet quenching mechanism and the gluon shadowing

total inelastic cross-section for Pb+Pb collisions at LHC ($\sigma_{\text{inel,Pb+Pb}}^{\text{tot}} = 8$ barn). The magnetic field has been set to $B = 0.5$ T. The GEANT3 package [10] has been used to track all the particles produced in the collision within the pseudorapidity range $|\eta| < 8$, and to simulate the detector signals and responses. Vertex reconstruction, particle tracking, and particle identification have been performed as described in [11].

The mean number of generator-level primary charged (both negative and positive) particles² per event within the pseudorapidity range $-0.9 < \eta < 0.9$ and for $0.15 < p_T < 4$ GeV/c is reported in Table 1 for the three different particle species of interest in this analysis (i.e. pions, kaons and protons). The average charged particle multiplicity per unit rapidity per event is $dN_{\text{ch}}/dy \sim 4500$. The p_T value of 4 GeV/c corresponds to the upper limit of the transverse momentum range of

Particle Species	Number of Primaries
π	6750
K	720
p	380

Table 1: Mean number of charged (both negative and positive) generator-level primaries per event generated in the pseudorapidity range $-0.9 < \eta < 0.9$, with transverse momentum $0.15 < p_T < 4$ GeV/c. The values refer to the sample of 300 HIJING central Pb+Pb events used for the results presented in this article.

interest for the event-by-event fluctuation analyses presented here (see Sec. 4.2, 4.3 and 4.4), while the pseudorapidity interval $-0.9 < \eta < 0.9$ reflects the fiducial acceptance of the ALICE central detectors which have been used in this study.

3. Particle Identification in ALICE

In the central rapidity region $-0.9 < \eta < 0.9$, inside the L3 magnet (providing the experiment with a weak solenoidal magnetic field $B = 0.2 - 0.5$ T), ALICE will be endowed with subdetectors specialized in tracking and identifying the particles produced in the collisions. Going outwards from the centre of the experiment, the innermost detector is the ITS (Inner Tracking System), which is a silicon detector mainly aimed at the reconstruction of the primary and the secondary vertices. Then, next to the ITS, the ALICE main tracking device, the TPC (Time Projection Chamber), will be installed, with a momentum resolution $\sigma(p)/p < 5\%$ up to 10 GeV/c. Both the ITS and the TPC will be able to perform Particle Identification for charged hadrons via dE/dx measurements in the low momentum region ($p \lesssim 1$ GeV/c). After the TPC, the Transition Radiation Detector (TRD), will concentrate mainly on the identification of high momentum electrons ($p \gtrsim 1$ GeV/c) in the central region, playing also an important role in the ALICE particle tracking. At 3.7 m from the centre of the experiment, the Time Of Flight (TOF) detector will be devoted to charged hadron identification in the intermediate momentum range ($0.5 \lesssim p \lesssim 4$ GeV/c). The central region will be

effect. In particular, as far as the jet quenching is concerned, the minimum p_T for a jet to interact with nuclear matter and the energy loss dE/dx of a gluon jet inside the excited matter have both been set to 2 GeV/c.

²A particle is defined here as *generator-level primary* if its generated production vertex is less than 1 μm from the generated interaction vertex.

also equipped with two detectors having partial azimuthal coverage: the HMPID (High Momentum Particle Identification Detector), a RICH detector which will carry out charged hadron identification in the high momentum range (up to $p \sim 3 - 5 \text{ GeV}/c$), and the PHOS (Photon Spectrometer), a crystal calorimeter for the detection of low energy photons. At large rapidity values, ALICE will be endowed with other detectors, namely the Muon Spectrometer, the Zero Degree Calorimeter (ZDC), the Photon Multiplicity Detector (PMD), the Forward Multiplicity Detector (FMD) and the V0 and T0 detectors (for more details see [12]).

The event-by-event fluctuation studies reported in the following rely on the excellent capabilities of the ALICE experiment in terms of Particle IDentification (PID). As a matter of fact, the ALICE experiment will be able to identify charged particles in a wide momentum range, from $\sim 0.1 \text{ GeV}/c$ up to a few GeV/c (and even more, up to a few tens of GeV/c , thanks to the TPC dE/dx measurements in the relativistic region [11]), taking advantage of the particle identification capabilities of the various detectors, each specifically designed to perform PID in some narrower momentum range, nearly complementary to the others. Besides, when some tracks are reconstructed simultaneously by different detectors, then a dedicated particle identification procedure can be applied, in order to combine all the available PID information.

For the analysis presented hereafter, the concern has been turned to the PID capabilities of the central tracking detectors ITS and TPC, and of the Time Of Flight detector. The ITS, TPC and TOF enter the common Bayesian-approach framework adopted by every ALICE detector performing PID, which allows to combine PID information of different nature, coming from different detectors, at the same time, with the advantage of being completely automatic. Moreover, this framework is able to make simultaneous use of signals distributed according to quite different probability density functions. For more details on ALICE particle identification, see [11].

For the present study, the PID signals from ITS, TPC and TOF have been combined in a logic “or” (ITS||TPC||TOF). This means that an identity is assigned to each particle provided that at least one of the three detectors has been able to perform particle identification on it. The main advantage of this approach is that it allows to have at its disposal the largest number of useful tracks for the E-by-E analysis. However, when only one PID signal is available, the level of contamination may rise, as it happens in the case of kaons at high p_T when only the TPC is able to provide a PID response.

3.1 Primary Track Selection

The analysis described hereafter has been carried out on reconstructed primary tracks. The primary track selection has been performed applying a χ^2 -cut which takes into account both the distance of the extrapolation of the tracks to the reconstructed primary vertex, and the covariance matrix of the track parameters. Figure 1 shows the efficiency $\varepsilon(\chi^2)$ of the primary track selection for the three particle species (π , K and p) in terms of the ratio between the number of reconstructed tracks which satisfy the χ^2 -cut provided that they are from generator-level primaries ($N(\chi^2|\text{prim})$), and the number of reconstructed generator-level primaries ($N(\text{prim})$),

$$\varepsilon(\chi^2) = \frac{N(\chi^2|\text{prim})}{N(\text{prim})}. \quad (3.1)$$

For all the three particle species, the efficiency of the χ^2 -cut levels at about 90% for transverse

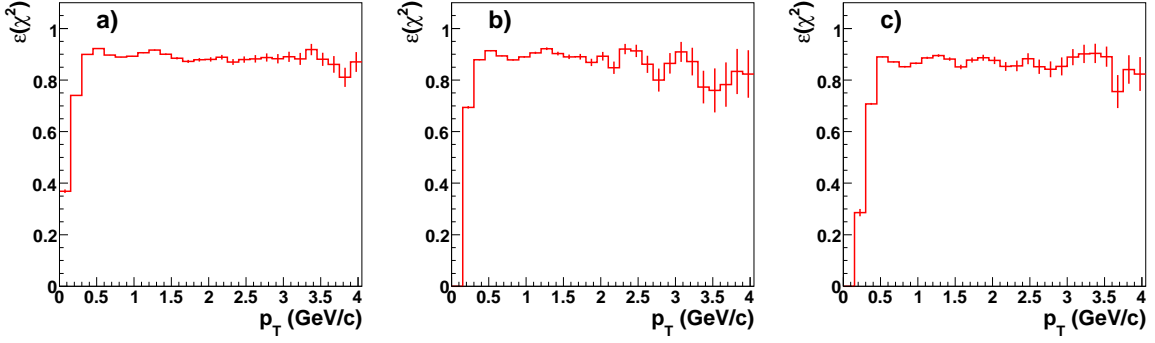


Figure 1: Efficiency of the χ^2 -cut for the three particle species (pions (a), kaons (b) and protons (c)).

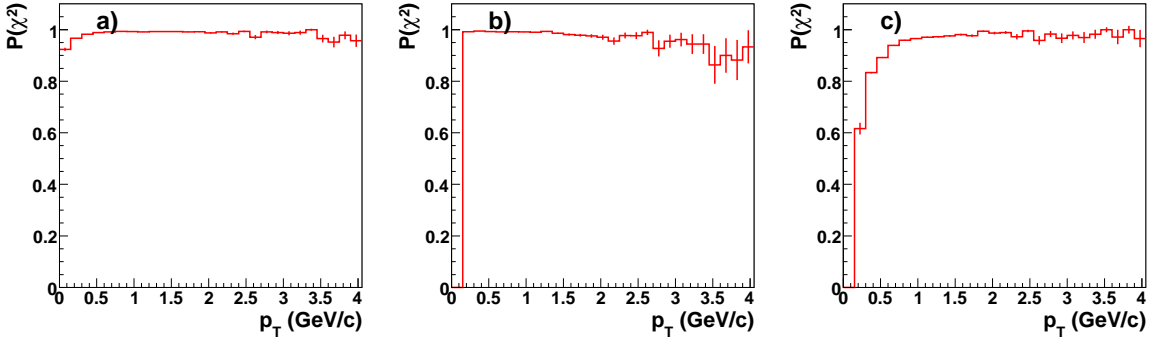


Figure 2: Purity of the χ^2 -cut for the three particle species (pions (a), kaons (b) and protons (c)).

momenta $p_T > 0.4$ GeV/c, being the $\sim 10\%$ loss being due to reconstruction defects.

On the other hand, the purity $P(\chi^2)$ of the χ^2 -cut (i.e. the fraction of reconstructed tracks in the selected sample which come from generator-level primary particles) can be defined in terms of the ratio of the number of reconstructed generator-level primary particles which satisfy the cut ($N(\text{prim}|\chi^2)$), over the total number of reconstructed tracks selected by the cut ($N(\chi^2)$),

$$P(\chi^2) = \frac{N(\text{prim}|\chi^2)}{N(\chi^2)}. \quad (3.2)$$

The results are shown in Fig. 2. As one can see, in the sample selected by the χ^2 -cut the contribution coming from secondaries (i.e. $1 - P(\chi^2)$) is of the order of a few percent for all the three species (π , K and p), over the whole momentum range. In the case of protons, at low p_T ($p_T < 1$ GeV/c) a drop in the purity of the χ^2 -cut can be observed, which is due to the contribution of secondary protons coming from Λ and Σ weak decays, as shown in Fig. 3. Here it is possible to observe that in the low momentum range ($p_T \lesssim 1$ GeV/c) about 10% of the total sample of reconstructed protons selected as primaries by the χ^2 -cut comes from Λ and Σ hyperons.

3.2 PID Results

Figure 4 shows the performance of the combined PID algorithm when applied to the primary tracks selected by the χ^2 -cut from the event sample, in terms of efficiency ϵ^{PID} and contamination

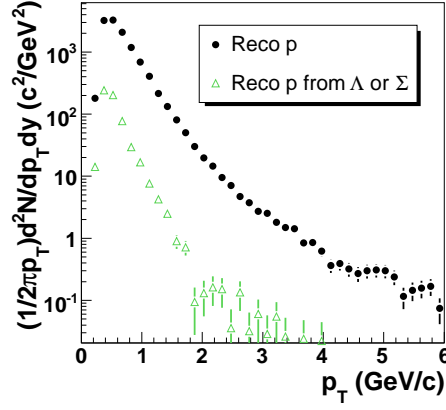


Figure 3: Transverse momentum spectra for reconstructed protons labelled as primaries by the χ^2 -cut (circles), and for the fraction of them coming from the weak decay of a Λ or Σ particle (triangles).

C^{PID} defined as:

$$\varepsilon^{\text{PID}}(i) = \frac{N_{\text{id}}^{\text{t}}(i)}{N(i)}, \quad C^{\text{PID}}(i) = \frac{N_{\text{id}}^{\text{w}}(i)}{N_{\text{id}}^{\text{t}}(i) + N_{\text{id}}^{\text{w}}(i)}, \quad (3.3)$$

$N(i)$ being the number of particles of type i ($i = \pi, K, p$) reconstructed by the central tracking, $N_{\text{id}}^{\text{t}}(i)$ the number of i -particles correctly identified, and $N_{\text{id}}^{\text{w}}(i)$ the number of non- i -particles misidentified as particles of type i . As one can see, as far as pions are concerned, the combined PID shows an efficiency which stays around 99%. On the other hand, the kaon efficiency varies between $\sim 70\%$ and $\sim 98\%$ in the low transverse momentum region ($0.15 < p_T < 0.75 \text{ GeV}/c$), and levels at a rather constant value $\varepsilon \sim 55\%$ up to $p_T < 3 \text{ GeV}/c$. At higher transverse momenta, a drop in the kaon efficiency occurs, due to the fact that the kaon identification suffers from a reduction in the separation power of the TOF detector. In the case of protons, at low momenta ($p_T < 1.3 \text{ GeV}/c$) the efficiency ranges from ~ 70 to $\sim 99\%$, while at intermediate and high p_T , it remains almost constant at $\sim 60\%$. The levelling of the efficiency for K and p for $p_T \gtrsim 1.3 \text{ GeV}/c$, where the Time Of Flight detector identification capabilities become crucial, reflects the TOF acceptance: because of the interactions with the TRD material in front of the Time Of Flight, only $\sim 50\%$ of the particles reconstructed up to the outer wall of the TPC arrive at the TOF sensitive surface, and are then identified by the TOF. In the case of pions this effect does not show up, since the TPC particle identification is such that at intermediate and high p_T most of the particles are identified as π .

As far as contamination is concerned, over the whole transverse momentum range for pions and protons, and up to $p_T \sim 2.5 \text{ GeV}/c$ for kaons, the fraction of misidentified particles ranges from few percent up to a maximum of $\sim 25\%$ (for kaons). Still in the case of kaons, the substantial increase of the contamination for $p_T > 2.5 \text{ GeV}/c$ is both due to a loss in the separation power of the TOF detector and to those particles identified by the TPC alone in the dE/dx relativistic rise region. Moreover, the peak at $p_T \sim 0.7 \text{ GeV}/c$ corresponds to the overlap of the π and K bands in the dE/dx vs p plane in the TPC.

Figure 5 shows the overall efficiency of the combined particle identification technique, defined as:

$$\varepsilon_{\text{ov}}(i) = \frac{N_{\text{id}}^{\text{t}}(i)}{N(i)_{\text{prim}}},$$

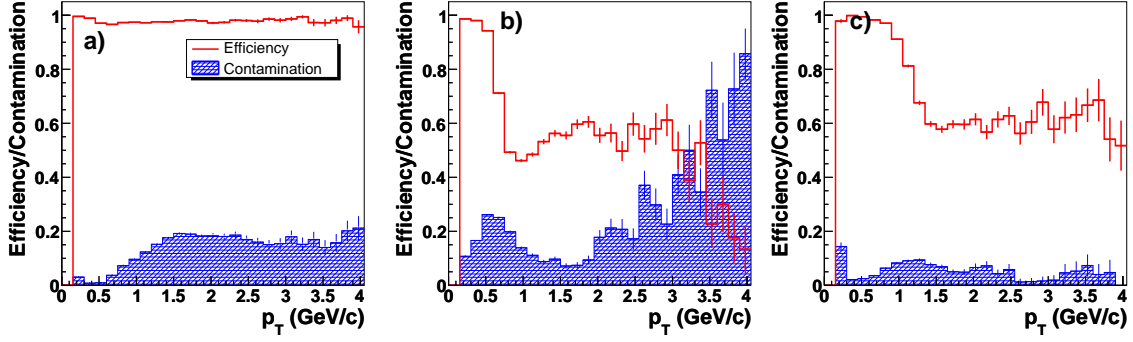


Figure 4: Efficiency and contamination for the combined ITS||TPC||TOF particle identification procedure applied to 300 HIJING central events for the three particle species: pions (a), kaons (b) and protons (c).

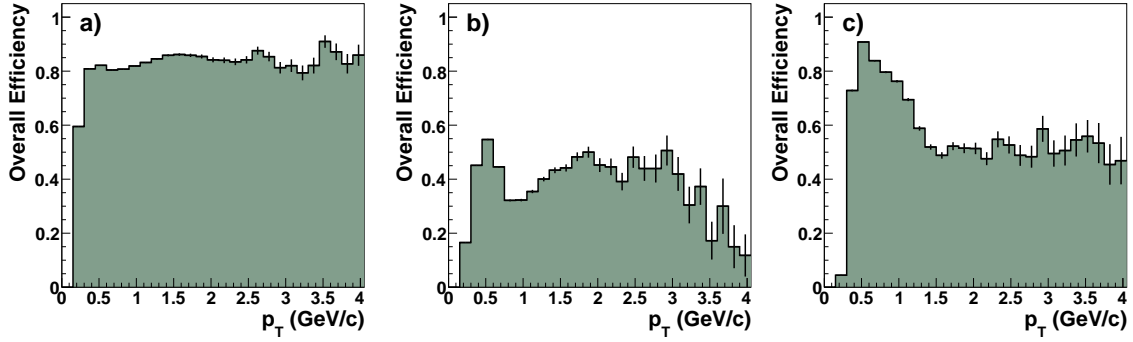


Figure 5: Overall efficiency for the combined ITS||TPC||TOF particle identification procedure applied to 300 HIJING central events for the three particle species: pions (a), kaons (b) and protons (c).

where $N(i)_{\text{prim}}$ is the number of generator-level primaries of type i in $|\eta| < 0.9$. Since ε_{ov} is calculated with respect to the generated primaries, it takes also into account various factors which affect the PID results, mainly the reconstruction efficiency (also in terms of the χ^2 -cut), the effects of dead zones and of particle decays and interactions. In the case of pions, it stays at an almost constant level of $\sim 80\%$, while for kaons it varies from $\sim 30\%$ to $\sim 50\%$ for $0.3 < p_T < 3.4$ GeV/c, decreasing in the highest transverse momentum region again mainly because of the loss in the TOF separation power. For what concerns protons, the overall efficiency in the low p_T region ($p_T \lesssim 0.5$ GeV/c) ranges from $\sim 75\%$ up to $\sim 90\%$, and then drops to $\sim 50\%$ already at $p_T \sim 1.3$ GeV/c (still as a consequence of the TOF acceptance).

As a summary, Table 2 quotes the efficiency, contamination and overall efficiency from the combined PID technique, integrated over the corresponding transverse momentum ranges for the three particle species.

For the purpose of this analysis, it is also meaningful to indicate the average number of particles of different species that can be identified per event by the combined PID technique. Table 3 quotes the mean number (over the 300 events) of pions, kaons and protons which are identified in a Pb+Pb central collision. As one can see, even in the case of kaons and protons, the number of identified particles is considerably high. This will make ALICE the first experiment able to perform

	π	K	p
efficiency	98%	78%	92%
contamination	3%	20%	5%
overall efficiency	74%	40%	70%

Table 2: Efficiency, contamination, and overall efficiency for π , K, and p using the combined PID technique, integrated over the momentum range $0.15 < p_T < 4$ GeV/c, within the pseudorapidity range $-0.9 < \eta < 0.9$ (see text for more details).

	π	K	p
N_{id}	5143	359	280
$N_{\text{id,true}}$	4988	285	267

Table 3: Average numbers of identified pions, kaons and protons per event. The “true” label refer to correctly identified particles.

event-by-event fluctuation analysis also for hadron species other than pions, with a highly efficient PID and over a wide momentum range.

4. Fluctuations in ALICE

The E-by-E fluctuation studies presented hereafter have been carried on starting from the identified hadron p_T spectra from the 300 HIJING event sample previously described. In the following sections, the analysis method adopted will be presented.

4.1 p_T Spectra

Figure 6 shows the transverse momentum spectra separately for pions, kaons and protons obtained for the 300 HIJING central event sample described in Sec. 2. The distributions labelled as *identified* have been obtained with the combined particle identification procedure presented in Sec. 3. The labels *true* and *wrong* refer to correctly identified and mis-identified particles, respectively. For each event, in order to recover the p_T spectra of the charged particles generated in the collision, the transverse momentum distributions of the identified hadrons have been corrected. Two correction factors have been applied. The first (ϵ) takes into account three “efficiency” contributions: *i*) the limited geometrical acceptance of the detectors (ϵ^{acc}), implying that not all the generated particles are reconstructed and therefore subject to the PID procedure discussed in Sec. 3; *ii*) the particle identification efficiency (ϵ^{PID}), implying that not all the particles to which the PID is applied are correctly identified; *iii*) the transverse momentum reconstruction efficiency (ϵ^{p_T}), implying that the reconstructed transverse momentum may differ from the generated one. The second correction factor (C) is instead due to the possible mis-identification of the charged hadrons (C^{PID}). From now on, the p_T distributions of the identified particles (“id”) corrected for both efficiency and contamination will be labelled as *reconstructed* (“R”) spectra. As a result, the

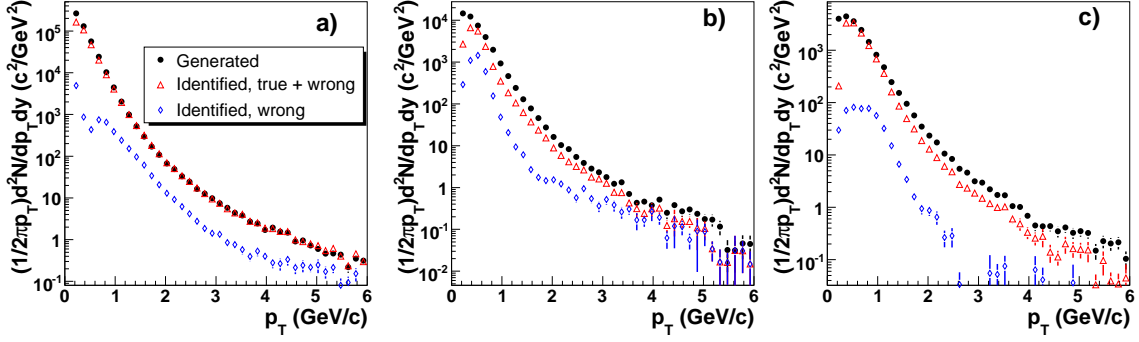


Figure 6: Transverse momentum pion (a), kaon (b) and proton (c) spectra for 300 HIJING central events.

relation:

$$\frac{d^2N}{dp_T dy}(\text{R}) = \frac{1}{\varepsilon} \times (1 - C) \times \frac{d^2N}{dp_T dy}(\text{id}),$$

$$\varepsilon = \varepsilon^{\text{acc}} \times \varepsilon^{\text{PID}} \times \varepsilon^{p_T}, \quad C = C^{\text{PID}}$$

holds true. The efficiency and contamination factors have been calculated considering the whole event sample under study.

4.2 $\overline{p_T}$ Measurements

From the corrected spectra described in Sec. 4.1, the event-wise mean transverse momentum can be extracted. This is one of first observables proposed to study the QGP phase transition, since fluctuations in $\overline{p_T}$ are sensitive to models describing nuclear collisions [5]. Moreover, if the system passes through the QCD critical point, a distortion (or even an enhancement) of the $\overline{p_T}$ distribution may occur [4, 5]. Figure 7 shows the distribution of the event-wise mean transverse momentum obtained for the 300 events of the HIJING Pb+Pb sample, for the three particle species π , K and p. The same combined PID algorithm as before has been used, and the correction factors have been applied. As one can see, the ALICE experiment statistical sensitivity for such analyses is of the order of $\sim 1\% \sim 4\%$ and $\sim 7\%$ for π , K, and p respectively. Table 4 summarizes the results. A good agreement can be observed among the $\langle \overline{p_T} \rangle$ values obtained considering the $\overline{p_T}$ distributions of the generated primaries, and the reconstructed ones. On the other hand, the widths of the distributions of the $\overline{p_T}$ for the generated spectra are smaller than those obtained from the reconstructed ones. This difference can be entirely understood in terms of the efficiency factors which relate the generated particle spectra to the reconstructed ones.

4.3 Temperature Measurements

One of the main parameters in describing the system produced in heavy-ion collisions is temperature. Since the matter produced at the very early stages of the collision is thought to reach at least local thermodynamic equilibrium, trying to understand whether a unique temperature can describe the freeze-out, or if temperature fluctuations occur from event to event is of great interest. Moreover, temperature is closely related to the total heat capacity of the system [4], and so to

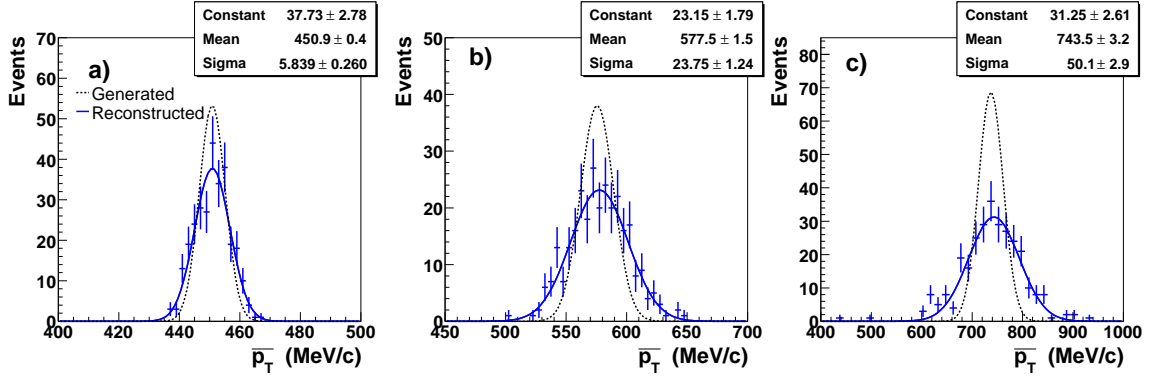


Figure 7: $\overline{p_T}$ distributions for reconstructed π (a), K (b) and p (c) spectra for 300 HIJING central events. The Gaussian fits of the $\overline{p_T}$ distributions from reconstructed and generated spectra are superimposed. The fit parameters obtained for $\overline{p_T}$ from reconstructed hadron spectra are reported in the top right panels.

	π	K	p
$\langle \overline{p_T} \rangle$ (MeV/c), G	450.9 ± 0.3	575.7 ± 0.8	737.2 ± 1.5
$\sigma(\overline{p_T})$ (MeV/c), G	4.3 ± 0.2	13.7 ± 0.8	24.5 ± 1.2
$\langle \overline{p_T} \rangle$ (MeV/c), R	450.9 ± 0.4	577.5 ± 1.5	743.5 ± 3.2
$\sigma(\overline{p_T})$ (MeV/c), R	5.8 ± 0.3	23.8 ± 1.2	50.1 ± 2.9

Table 4: $\langle \overline{p_T} \rangle$ values obtained from the Gaussian fits of the $\overline{p_T}$ distributions for generated (G) and reconstructed (R) π , K and p. The σ of the Gaussian fits are quoted as well.

the specific heat, the behaviour of which depends on the existence (and on the nature) of a phase transition.

Experimentally, temperature can be extracted from the slope parameters of p_T spectra. So, temperature fluctuations can be indirectly studied through the fluctuations in the inverse slope parameter derived from the transverse momentum spectra.

From the shape of the spectra of Fig. 6 it is possible to infer that up to $p_T \sim 2$ GeV/c an exponential fit to the p_T distributions would be a reasonable choice. For this reason, an event-by-event fitting procedure has been applied to the event sample for the three particle species in the transverse momentum range $0.25 < p_T < 2$ GeV/c, which sits below the high p_T region where the exponential form of the p_T spectra is no more expected [13, 14, 15], and which allows a good compromise between the efficiency and the contamination of the combined PID algorithm. For the transverse momentum spectra an exponential function of the form:

$$\frac{1}{2\pi p_T} \frac{d^2 N}{dp_T dy} \propto \exp\left(-\frac{p_T}{T}\right), \quad (4.1)$$

has been used, where the inverse slope parameter T is the so-called “effective” temperature, related in fact to the kinetic freeze-out temperature and to the mean transverse flow velocity [16, 17]. To be noted that even if the kinetic freeze-out temperature is unique for all the particle species, the “effective” freeze-out temperature is not, because of the effects of the transverse flow. Figure 8

shows the reconstructed p_T spectra (triangles) and the results of the fitting procedure (solid line) for the three particle species for one of the simulated events. The generated transverse momentum spectra (circles) are shown as well, as a reference for the reconstructed spectra (the correction being as described in Sec. 4.1).

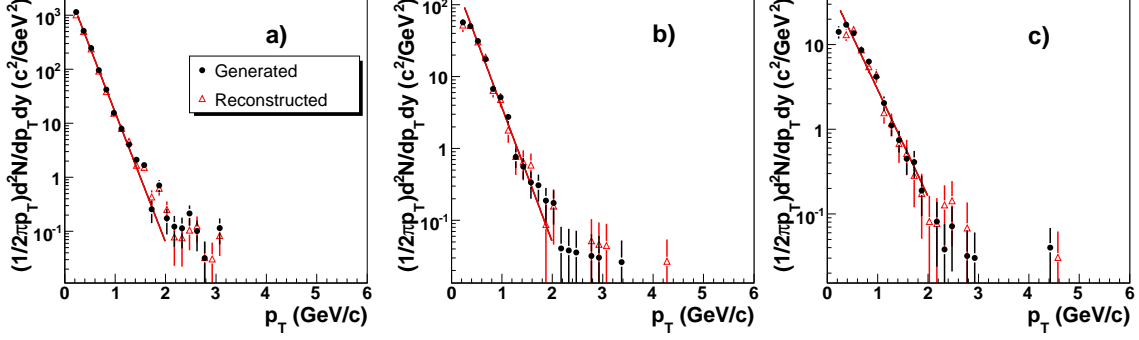


Figure 8: Reconstructed (see text) p_T pion (a), kaon (b) and proton (c) spectra for a single HIJING central event with the exponential fits described in the text superimposed. The generated spectra are drawn as well.

4.3.1 Measurement of the Inverse Slope Parameter

Figure 9 shows the distributions of the inverse slope parameters obtained for the 300 HIJING reference event sample, for pions, kaons, and protons. The results of the Gaussian fits performed over the distributions of the inverse slope parameters extracted from the reconstructed hadron p_T spectra are shown, together with those from the generated p_T spectra. Table 5 summarizes the results. Here, even if the mean inverse slope values obtained considering the p_T distributions of the generated primaries, and the reconstructed ones agree with each other within the errors, a small difference remains, probably due to the assumption of an exponential form used in the fitting procedure of the spectra which, in fact, are not rigorously exponential. As in the case of $\overline{p_T}$ measurements, the distributions of the inverse slope parameter for the generated p_T spectra are narrower than those obtained from the reconstructed ones, as a consequence of the use of the efficiency factors to correct the particle spectra.

	π	K	p
$\langle T \rangle$ (MeV/c), G	181.5 ± 0.2	227.8 ± 0.6	301.0 ± 0.9
$\sigma(T)$ (MeV/c), G	2.7 ± 0.1	9.4 ± 0.4	15.2 ± 0.7
$\langle T \rangle$ (MeV/c), R	181.9 ± 0.2	226.4 ± 0.9	302.5 ± 1.5
$\sigma(T)$ (MeV/c), R	3.2 ± 0.2	12.7 ± 0.7	21.1 ± 1.3

Table 5: Mean inverse slope parameter T values obtained from the Gaussian fits of the T distributions for generated (G) and reconstructed (R) π , K and p spectra. The σ of the Gaussian fits are quoted as well.

As one can see, the ALICE precision in terms of inverse slope parameter measurement is expected to be of the order of 2%, 6% and 7% for identified pions, kaons and protons respectively (see Table 5).

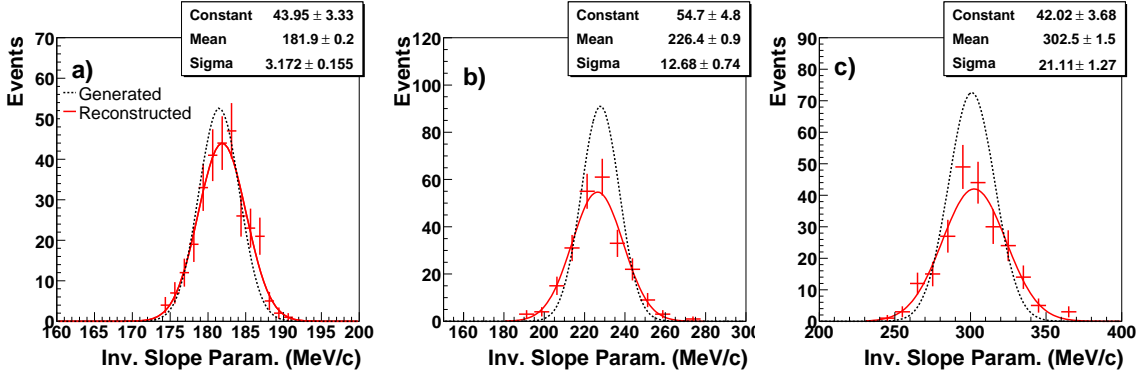


Figure 9: Inverse slope parameter T distributions for reconstructed π (a), K (b) and p (c) spectra. The Gaussian fits of the T distributions from reconstructed and generated spectra are superimposed. The fit parameters obtained for reconstructed hadron spectra are reported in the top right panels.

4.3.2 Evaluation of Systematics

The uncertainty on the results from event-by-event studies is largely due to the limited number of particles which are taken into account, i.e. it has a statistical origin. Apart from these statistical errors, there are other sources of uncertainties, such as the understanding of the geometrical acceptance of the detectors, the decays, the effects of multiple scattering, and nuclear interactions with the materials in the detectors. Moreover, p_T cuts applied in the PID algorithm, or in the analysis, and the efficiency and contamination of the particle identification procedure can affect the observed particle spectra.

In order to estimate to what extent the systematic errors on the efficiency and contamination correction factors could affect the results, the correction factors have been varied by 10%. Notice that this choice is arbitrary (representing a reasonable guess for what is expected for the ALICE experiment), and that a more precise estimate of the actual level of the systematic errors has still to be carried out in a dedicated study. This study has shown that no significant change in the mean values of the distributions occurs, either in the case of a 10% variation of the efficiency factor or in that of a similar variation of the contamination factor. Similarly, the σ of the distributions, reflecting the precision with which the inverse slope parameter value can be known, are only slightly affected by systematic uncertainties.

4.4 Measurements of Particle Ratios

Besides the event-by-event fluctuation analysis based on the mean transverse momentum $\overline{p_T}$ and on the inverse slope parameter T , the particle identification capabilities of the ALICE experiment will make it possible to study particle ratios, in particular K/ π and p/ π ratios. Figure 10 shows the result of the E-by-E particle ratio study performed on the 300 HIJING reference events. As in the case of $\overline{p_T}$ and T fluctuations, the particle identification has been performed with the combined PID algorithm (see Sec. 3), and the identified particle spectra have been corrected for efficiency and contamination as described in Sec. 4.1. The Gaussian fits to the reconstructed particle ratio distributions are superimposed, as well as the Gaussian fits to the generated ones. Table 6 quotes the results of the fits for the generated and reconstructed particles. As one can see, the results agree with each other within the errors.

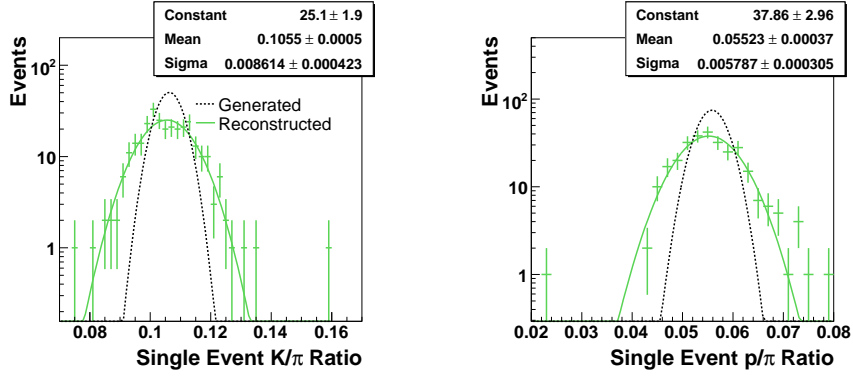


Figure 10: K/π and p/π particle ratios for generated and reconstructed particles in the reference event sample. The parameters of the fit to the reconstructed particle ratios are reported in the top right panels.

Particle Ratio	K/π	p/π
$\langle \text{Ratio} \rangle, G$	0.1063 ± 0.0003	0.0558 ± 0.0002
$\sigma(\text{Ratio}), G$	0.0045 ± 0.0003	0.0031 ± 0.0001
$\langle \text{Ratio} \rangle, R$	0.1055 ± 0.0005	0.0552 ± 0.0004
$\sigma(\text{Ratio}), R$	0.0086 ± 0.0004	0.0058 ± 0.0003

Table 6: Gaussian fit results for the distributions of the K/π and p/π particle ratios for generated (G) and reconstructed (R) particles.

The results show that the ALICE detector will be able to measure particle ratios with a statistical uncertainty of the order of $\sim 8\%$ and $\sim 11\%$ for K/π and p/π respectively.

5. Summary and Conclusions

It has been shown that thanks to the very high particle yield per event and to an excellent PID capability, the ALICE experiment will be able to study fluctuations by measuring the identified particle spectra for the three charged hadron species π , K and p. The analyses of \overline{pT} and inverse slope parameter T , and of the particle ratios K/π and p/π on an event-by-event basis have been presented. The statistical fluctuations are expected to be of the order of a few percent for all the three particle species, π , K, and p both for \overline{pT} and T measurements. As far as particle ratios K/π and p/π are concerned, the statistical fluctuations are again expected at the level of some percent. Any other contribution from dynamical fluctuations due to new physics may result in an increase of the observed values, or even in a distortion (non-Gaussian shapes) of the distributions.

It is fair to mention that the results presented herein strongly depend on the assumed charged particle multiplicity per unit rapidity, dN_{ch}/dy . The Monte Carlo simulation with the HIJING generator used for the analysis presented so far provides $dN_{ch}/dy \sim 4500$ (central Pb+Pb collisions). The range of $dN_{ch}/dy \sim 1500 - 2000$ suggested by the most recent studies (considering also the results from RHIC) [19, 20] would imply a reduction by a factor $\sim 2 - 3$ in the observed number of charged particles, and, in turn, an increase by a factor $\sim \sqrt{2} - \sqrt{3}$ in the uncertainties on the E-by-E

determination of the mean transverse momentum, of the inverse slope parameters and of particle ratios. Nonetheless, even in the case of a lower multiplicity, the number of identified π , K and p would still remain high enough to perform studies on an event-by-event basis.

On the other hand, a lower charged particle multiplicity would allow to obtain a better performance as far as track reconstruction and particle identification are concerned (see [11]), improving the quality of the particle sample on which the E-by-E analysis is carried on both in terms of efficiency and purity. Moreover, if at $p_T \gtrsim 1.5$ GeV/c the relative particle yields of π , K and p become comparable (as suggested from recent results at RHIC [18]), the PID performance would substantially improve, especially for kaons and protons. As a consequence, the uncertainties on $\overline{p_T}$, inverse slope parameter and particle ratio measurements are expected to be reduced, compensating at least in part the increase due to the lower dN_{ch}/dy .

Finally, it is also worth to remark that a more precise and detailed E-by-E study will be possible using the much larger number of events from the ALICE Physics Data Challenge 2006. It is also foreseen to introduce dynamical effects in the simulation in order to quantify their impact on E-by-E fluctuation analyses.

References

- [1] M. M. Aggarwal et al. (WA98 Collaboration), Phys. Rev. C65 (2002) 054912.
- [2] M. Gaździcki and S. Mrówczyński, Z. Phys. C54 (1992) 127.
- [3] D. P. Mahapatra, B. Mohanty and S. C. Phatak, Int. J. Mod. Phys. A17 (2002) 675.
- [4] L. Stodolsky, Phys. Rev. Lett. 75 (1995) 1044;
- [5] E. V. Shuryak, Phys. Lett. B423 (1998) 9.
- [6] J. Zaranek, Phys. Rev. C66 (2002) 024905;
S. Mrówczyński, Phys. Rev. C66 (2002) 024904.
- [7] Qing-jun Liu and T. A. Trainor, Phys. Lett. B567 (2003) 184;
M. J. Tannenbaum et al. (PHENIX Collaboration), J. Phys. G30 (2004) S1367.
- [8] B. Mohanty and J. Serreau, Phys. Rept 414 (2005) 263.
- [9] X. N. Wang et al., Phys. Rev. D44 (1991) 3521;
X. N. Wang et al., Phys. Rev. Lett. 68 (1992) 1480;
M. Gyulassy and X. N. Wang, Comput. Phys. Commun. 83 (1994) 307;
OSCAR, Open Standard Code and Routines, <http://nt3.phys.columbia.edu/OSCAR>.
- [10] R. Brun, F. Bruyant, A. Mc Pherson and P. Zancarini, Geant3 User Guide, CERN Data Handling Division DD/EE/84-1.
- [11] ALICE Collaboration, ALICE: Physics Performance Report Volume II (2005) CERN/LHCC 2005-030, Eds. B. Alessandro et al. (ALICE Collaboration), J. Phys. G: Nucl. Part. Phys. 32 (2006) 1295.
- [12] ALICE Collaboration, ALICE: Physics Performance Report Volume I (2003) CERN/LHCC 2003-049, Eds. F. Carminati et al. (ALICE Collaboration), J. Phys. G: Nucl. Part. Phys. 30 (2004) 1517.

- [13] PHENIX Collaboration, K. Adcox et al., Phys. Rev. C69 (2004) 024904.
- [14] D. Teaney, J. Laurent and E. V. Shuryak, nucl-th/0110037 (2001);
D. Teaney, J. Laurent and E. V. Shuryak, Phys. Rev. Lett. 86 (2001) 4783.
- [15] P. F. Kolb and R. Rapp, Phys. Rev. C67 (2003) 044903.
- [16] E. Schnedermann, J. Sollfrank and U. Heinz, Phys. Rev. C48 (1993) 2462.
- [17] T. Csörgo and B. Lorstad Phys. rev. C54 (1996) 1390.
- [18] PHENIX Collaboration, S. S. Adler et al., Phys. Rev. C69 (2004) 034909.
- [19] K. J. Eskola, P. V. Ruuskanen, S. S. Rasanen and K. Tuominen, Nucl. Phys. B570 (2000) 379.
- [20] M. Nardi, J. Phys. Conf. Ser. 5 (2005) 148.